# Multifunctional Nanoparticles Biosynthesized From Carica Papaya Seeds: Characterization And Application In Antibacterial, Bio-Flocculating, And Dye Degradation Processes.

# Bukola Christianah Adebayo-Tayo, Eniola Anuoluwapo Dawodu, Olusola Ademola Olaniyi, And Oladeji Aderibigbe Ajani

Department Of Microbiology, University Of Ibadan, Ibadan, Oyo State, Nigeria
Department Of Mathematics And Computer Science, University Of North Carolina, Pembroke, USA. Federal
Medical Center, Old N. North Carolina HWY 75, Burner, NC 27509

#### Abstracts

**Background**: Green synthesis methods utilizing plant extracts offer a sustainable approach to producing silver and iron nanoparticles with diverse applications. This study aimed to synthesize silver (PESNPs) and magnetic (PEMNPs) nanoparticles using Carica papaya seed extracts and comprehensively characterize them to elucidate their properties and potential applications.

Materials and Methods: Silver and magnetic nanoparticles biosynthesized using Carica papaya seed extracts as a bio-reducing agent were characterized using UV-Vis spectroscopy, FTIR, XRD, SEM, TEM, EDX, and TGA. UV-Vis spectroscopy and the antibacterial, dye decolouration and bioflocculating potential were evaluated.

Results: Characteristic absorption peaks at 500 nm was observed for PESNPs and 400 nm for PEMNPs, indicative of their synthesis and Plasmon resonance. Hydroxyl, nitriles, carbonyl, aromatic, ether, and amine were the major functional groups present in PESNPs and PEMNPs which were responsible for the bioreduction and bio-oxidation process. XRD patterns confirmed crystalline structures with 4 peaks and 8 peaks PESNPs and PEMNPs respectively while PESNPs was spherical with a more rhombus-like shape and PEMNPs was circular but with uneven edges. EDX analysis confirmed the presence of silver and iron as the predominant metals which confirm the purity and highlight successful nanoparticle synthesis. TGA analysis demonstrated thermal stability up to 600°C for PESNPs and 300°C for PEMNPs. Antibacterial assays revealed the potent activity of PESNPs having higher antibacterial efficiency against the test isolates compared to PEMNPs. Salmonella typhimurium had the highest susceptibility (12.0 mm and 3.0 mm) to PESNPs and PEMNPs. PESNPs, higher than PEMNPs, exhibited 63.71 and 67.45 % efficient reduction of Congo red and methylene blue suggesting potential for wastewater treatment applications. Moreover, PESNPs had the highest bioflocculating potential of 87.80 % compared to PEMNPs with the bio-flocculating potential of 87.40 % at 24 hrs. Conclusion: The biosynthesized Carica papaya seed silver and magnetic nanoparticles had antibacterial, dye decolourization, and bio-flocculating efficacy.

**Keywords:** Nanoparticles, Biosynthesis, Carica papaya, Bio-flocculation, Antibacterial activity

Date of Submission: 04-11-2025

Date of Acceptance: 14-11-2025

#### I. Introduction

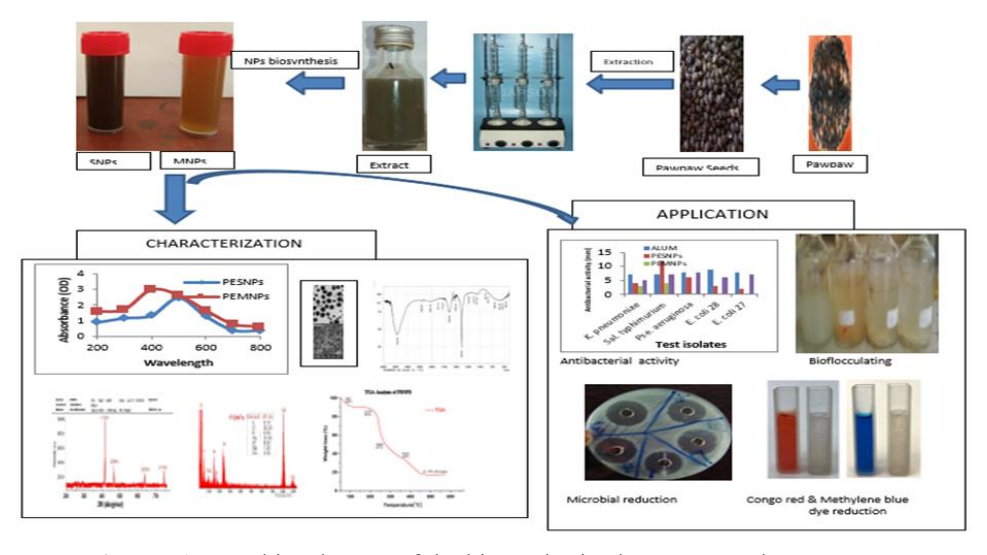
The revolution in nanotechnology has led to a significant historical turning point. Nanotechnology encompasses the development, manipulation, and visualization of nanostructures with sizes between 1 and 100 nm (Alharbi et al., 2022). Kupusamy et al. (2016), state that nanoparticles have diverse features and significant promise for use in several sectors such as medicine, nutrition, and energy. Thus, the manufacturing of environmentally friendly nanoparticles is considered a fundamental aspect for the future generation to manage different ailments (Cruz et al., 2010). Nanoscale particles have superior properties and less coordination compared to bulk materials due to atomic interactions on their surface. Nanoparticles can be made of either metals or nonmetals based on their basic structures. Metallic nanoparticles are mostly composed of magnetic elements such as cobalt and nickel, as well as silver, copper, gold, and semiconducting elements. Non-metallic nanoparticles primarily consist of carbon-based compounds. Metallic nanoparticles have been extensively studied because of their distinctive electrical, catalytic, and optical capabilities (Bharathi et al., 2018).

One of the most significant contributors to environmental pollution is organic dyes, commonly discharged by industries such as textiles, pulp and paper, cosmetics, plastics, food processing, pharmaceuticals, and others. Due to their complex chemical composition, these dyes exhibit remarkable stability, posing severe threats to ecological systems and environments, particularly aquatic ecosystems (Raina et al., 2020). Hence, there is a critical imperative to mitigate environmental contamination by ensuring the complete removal of dyes before industrial effluent discharges into water bodies. The elimination of these dyes from wastewater stands as a paramount challenge in the sector of environmental management. In recent years, the investigation into nanoparticles (NPs) has gained considerable traction, driven by their distinctive properties (Groiss et al., 2017). Capitalizing on this eco-friendly approach, diverse types of NPs have been synthesized (Dhar et al., 2021). Among these, Fe<sub>2</sub>O<sub>3</sub>-NPs, a subset of iron oxide nanoparticles, have garnered significant attention owing to their remarkable attributes, including excellent solubility in solutions, robust binding capabilities, and magnetic properties. Magnetic NPs can be magnetized through an external magnetic field and exhibit superparamagnetism or zero magnetization in its absence. Ranging in size from 2 to 20 nm, this characteristic renders magnetic nanoparticles in solutions exceptionally stable. Consequently, these unique characteristics have rendered magnetic nanoparticles indispensable across a wide array of industries, encompassing biomedicine, healthcare, environmental remediation, energy, defense and aerospace, construction, automotive, textiles, and electronics (Dash et al., 2019).

Biologically synthesized nanomaterial's derived from natural sources such as flowers, leaves, or seeds have potential for diverse applications spanning medical diagnostics, therapeutic interventions, the development of surgical Nano devices, and the manufacturing of commercial products (Bar *et al.*, 2009). Within plant crude extracts, newly discovered secondary metabolites encompass phenolic acids, flavonoids, alkaloids, and terpenoids. These compounds play a pivotal role in the reduction of ions to yield bulk metallic nanoparticles (Aromal and Philip, 2012). As outlined by Kupusamy *et al.* (2016), the ongoing redox reactions mediated by both primary and secondary metabolites contribute to the eco-friendly production of nanoparticles.

Carica papaya, commonly known as Papaya, Paw Paw, Kates, or Papaw, belongs to the Caricaceae family and is recognized among medicinal herbs. The bark, leaves, and fruits of *C. papaya* are utilized medicinally to address a wide array of ailments including syphilis, gonorrhea, cutaneous tubercles, warts, corns, constipation, amenorrhea, general debility, sinusitis, eczema, hypertension, dyspepsia, cancerous growth, diabetes, malaria, as well as to stimulate reproductive organs and expel worms (Aravind *et al.*, 2013; Sinhalagoda *et al.*, 2013). Recent research highlights the protective effects of *C. papaya* fruit extract against acrylamide toxicity in rats, attributed to its immunostimulant and antioxidant properties (Kadry, 2012). Rich in proteolytic enzymes, phenols, and vitamins, extracts from the fruit and leaves of *C. papaya* exhibit potent antibacterial properties and serve as effective antioxidants (Banala *et al.*, 2015).

The black seeds of Pawpaw, often overlooked due to the focus on the meaty pulp, are a rich source of micronutrients and possess antibacterial, anti-cancer, and other beneficial properties. Recognizing their potential, there is growing interest in exploring the possible applications of these seeds in nanotechnology and various other fields (Saba and Pattan, 2022). This study is aimed at utilizing the methanol extract of *C. papaya* seeds as a bio-reducing agent and nanocarrier for the biosynthesis of silver and magnetic nanoparticles. The study also involved characterizing the nanoparticles and assessing their antibacterial efficacy in vitro, as well as evaluating their capacity for dye reduction, heavy metal reduction, and bio-flocculation.



Figures 1: Graphic Abstract of the biosynthesized PESNPs and PEMNPs

#### II. Materials And Methods

#### **Collection of Plant Material and Cultures**

The pawpaw (*C. papaya*) used for this study was locally purchased from the market and authenticated at the Department of Botany, herbarium, University of Botany. Test microorganisms; *Klebisella pneumonia*, *Escherichia coli*, *Salmonella typhimurium*, and *Pseudomonas aeruginosa* were obtained from the Department of Microbiology, Faculty of Science at the University of Ibadan.

#### **Sample Preparation and Extraction for Plant Samples**

C. papaya seeds were subjected to air drying until complete removal of moisture, followed by finely grinding the dried seeds into a powder. This powder was subsequently immersed in 70% methanol and allowed to macerate at room temperature for 3 days to enhance the extraction of diverse active compounds present within the seeds. Following maceration, the mixture underwent centrifugation at 2500 rpm for 5 minutes, facilitating the separation of the supernatant. The supernatant was further purified by filtration to eliminate any solid residues. Finally, the solvent was evaporated from the extract using a rotary evaporator to yield the desired extract.

### Production of silver and magnetic nanoparticles

To synthesize silver nanoparticles (SNPs), a green-approach method was employed (Adebayo-Tayo et al., 2022). The metal precursor utilized for the synthesis of SNPs was silver nitrate (AgNO<sub>3</sub>). 5 g of the plant extract was dissolved in 100 mL of de-ionized water to create a stock solution. Subsequently, 5 mL of this stock solution was added to 20 mL of a 1M solution of AgNO<sub>3</sub>. The resultant mixture was then exposed to sunlight, facilitating the bio-reduction of AgNO<sub>3</sub> by the plant extracts into Ag<sup>o</sup> ions. The formation of nanoparticles was confirmed through visual observation, primarily noting color changes, followed by comprehensive characterization.

Similarly, for the synthesis of iron nanoparticles (FeNPs), a green-approach method was adopted. The metal precursor employed for FeNPs synthesis was iron oxide (Fe<sub>2</sub>O<sub>3</sub>). 5 grams of the plant extract were dissolved in 100 mL of de-ionized water to obtain a stock solution. Subsequently, 5 mL of this stock solution was added to 20 mL of a 1M solution of iron oxide (Fe<sub>2</sub>O<sub>3</sub>). The mixture was then exposed to sunlight for 12 hours to facilitate sun-induced nanoparticle production. Similar to the silver nanoparticles, confirmation of nanoparticle formation was achieved through physical observation, particularly color changes, followed by detailed characterization.

# **Characterization of Biosynthesized Nanoparticles**

# UV-Visible Spectroscopy of the Biosynthesized Nanoparticles

Silver and magnetic nanoparticles were characterized using a UV-Vis spectrophotometer with a scanning range of the samples was 200–800 nm at a scan speed of 480 nm/min (Mulvaney, 1996). The data in the spectrophotometer were recorded.

# Fourier Transform Infrared Spectroscopy (FT-IR) of the Biosynthesized Nanoparticles

The sample was centrifuged at 14,000 rpm to separate the supernatant, which was discarded and replaced with deionized water to re-suspend the nanoparticles (Suryawanshi and Vidyasagar, 2019). This washing step was repeated three times to ensure purity by removing unbound compounds. The purified nanoparticle precipitate was dried and ground with potassium bromide to form pellets. These pellets were analyzed using a Nicolet IR 200 spectrometer (Thermo Electron Corp, Madison, WI, USA) to determine the properties of the synthesized nanoparticles.

# X-ray diffraction (XRD) of the Biosynthesized Nanoparticles

The powdered nanoparticle samples were pelletized, sieved to 0.074 mm, and placed on an aluminum alloy grid for gentle hand compaction (Abdallah, and Hassan, 2020). Each sample was analyzed using a Rigaku D/Max-III C X-ray diffractometer with CuKa radiation at 40 kV and 20 mA. Scans were performed at  $20^{\circ}$ /min over a  $2^{\circ}$  to  $50^{\circ}$  range at room temperature.

#### Scanning Electron Microscopy (SEM) of the Biosynthesized Nanoparticles

The process involved mounting the nanoparticle specimens onto carbon-coated stubs and subsequently applying a gold coating using an Eiko IB3 ION coater (Abdallah et al., 2020). Following this preparation, SEM micrographs were acquired using a JEOL JSM-7800F field emission SEM to examine the size and morphology (shape) of the silver and magnetic bio-flocculant nanoparticles. Operating under high vacuum (HV) mode at a voltage of 10 kV, the SEM utilized various detectors, including secondary electron and semiconductor

backscattered electron (BSE) detectors of Quad type. Imaging was conducted at magnifications of 20, 50, and 100 µm to provide a comprehensive understanding of the nanoparticle characteristics.

#### Transmission Electron Microscopy (TEM) of the Biosynthesized Nanoparticles

The nanoparticles were prepared for TEM observation by dispersing them onto copper grids coated with a holey carbon film (Abdallah et al., 2020). The average particle size of both silver and magnetic bio-flocculant nanoparticles was determined through TEM measurements conducted in triplicate. The morphology and size of the silver and magnetic nanoparticles were assessed using a JEM-ARM200F-G transmission electron microscope.

#### Energy Dispersive X-ray (EDX) of the Biosynthesized Nanoparticles

Energy dispersive X-ray spectroscopy (EDX) analysis was conducted to validate the conversion of silver and ferric ions within the silver and magnetic nanoparticles into elemental silver and iron, respectively (Suryawanshi and Vidyasagar, 2019). This analysis was carried out using a Philips CM200 TEM operating at 200 kV. For sample preparation, the nanoparticles were dispersed onto copper grids coated with a holey carbon film. A selected micrograph obtained from TEM was coupled with an Oxford SDD X-MAX EDX system to determine the elemental compositions of the biosynthesized silver and magnetic nanoparticles.

#### Thermogravimetric Analysis (TGA) of the Biosynthesized Nanoparticles

Thermo-gravimetric analysis was conducted on silver and magnetic nanoparticles to evaluate thermal stability from 100°C to 600°C at a heating rate of 10°C/min under nitrogen flow (Suryawanshi and Vidyasagar, 2019). The nanoparticles were placed on a tared crucible on the sample platform of an STA 449/C Jupiter analyzer. Upon starting, the instrument heated and continuously weighed the sample to monitor changes. This setup enabled precise assessment of the nanoparticles' thermal behavior.

# Antimicrobial susceptibility test for the nanoparticle

Bacterial isolates were cultured on nutrient agar and standardized with the 0.5 McFarland standard (Wu, and Ye, 2007). Antimicrobial activity of nanoparticles was tested using the agar-well diffusion method by swabbing bacteria on agar, boring holes, and adding nanoparticles and streptomycin as control. Plates were incubated at 37°C for 24 hours before evaluation.

#### Determination of bio-flocculating potential of the C. papaya extract

The flocculation rate was determined using a 4 g/L kaolin suspension following Nkosinathi et al. (2020). In each 250 mL flask, 100 mL kaolin suspension was mixed with 2 mL culture supernatant and 3 mL of 1% CaCl<sub>2</sub>, shaken for 60 seconds, then left to settle for 5 minutes. A control without bio-flocculant was prepared similarly. After 2 hours, turbidity of the upper layer was measured at 550 nm using a spectrophotometer. The flocculation rate was estimated based on the reduction in turbidity compared to the control sample

Flocculation rate = 
$$(A - B/A) x 100$$

Where A and B stand for the optical densities of the control and the sample at 550 nm, respectively, the Triplicate of the experiment was performed and the mean value was determined.

#### Dye reduction potential of the nanoparticles

Methylene blue and Congo red dyes were prepared by dissolving 0.4g in 1000 mL distilled water (Dharshini et al., 2021). To test removal efficiency, 2 mL of nanoparticle stock was added to 100 mL dye solution, shaken for 30 minutes, then left to stand for 2 hours for flocculation. The supernatant was collected afterward for analysis at each dye's maximum wavelength. The removal efficiency (RE) was calculated using the formula:

$$RE (\%) = (Co - C1/Co) x 100$$

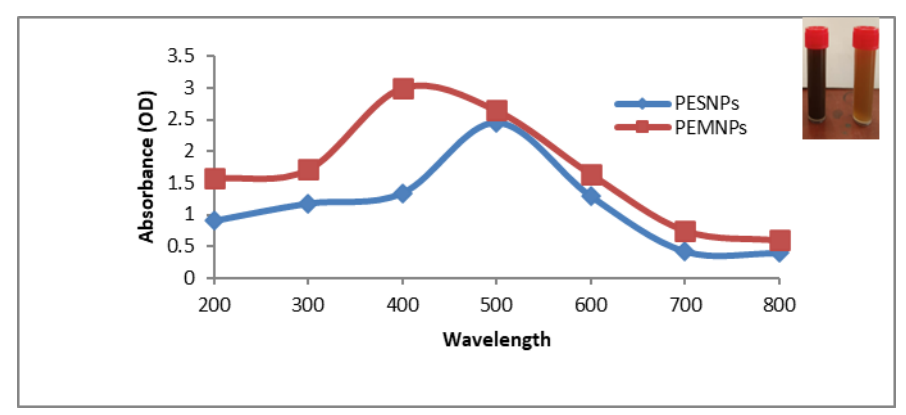
Where  $C_0$  is the initial value and  $C_1$  is the value after the flocculation treatment (Nkosinathi *et al.*, 2020).

#### III. Results

The initial observation was the change in color of the solution. It turned dark red for silver nanoparticles and dark blue for iron nanoparticles, indicating the production of silver and magnetic nanoparticles, respectively. The intensity of the color deepened over time in sunlight.

The biosynthesized PESNPs and PEMNPs were assessed by monitoring the reduction of metal ions through absorbance measurements across a wavelength range from 200 nm to 800 nm using a UV-Vis spectrophotometer. The UV-vis spectra of the biosynthesized PESNPs and PEMNPs are depicted in Figures 2.

The PESNPs exhibited a UV-visible maximum peak at a wavelength of 500 nm, with the highest surface Plasmon Resonance (SPR) peak absorbance recorded at 2.456. Different peak absorbance's was observed the biosynthesized PESNPs and PEMNPs. This peak absorbance indicates the successful conversion of Ag<sup>+</sup> ions to silver nanoparticles. On the other hand, the PEMNPs displayed a maximum absorbance at 400 nm, with the highest surface Plasmon Resonance (SPR) peak absorbance measured at 2.918. This observation confirms the presence of biosynthesized magnetic nanoparticles in the reaction mixture. The UV-vis spectra provide clear evidence of the formation of silver and magnetic nanoparticles, as indicated by the characteristic absorbance peaks observed at their respective wavelengths.



Figures 2: UV-Visible Spectra of a) PESNPs and b) PEMNPs

The FTIR analysis was performed to identify the potential biomolecules in PESNPs and PEMNPs which are responsible for the bio-reduction and capping of the biosynthesized nanoparticles by characterizing the functional groups present on the surface of the nanoparticles. Figures 3a and b show the FTIR spectrum of the biosynthesized nanoparticles and the spectra were measured at wave number 4400 − 350 cm<sup>-1</sup>. PESNPs have 6 absorption peaks ranging from a wavelength of 3487.00 to 459.00 cm<sup>-1</sup> which indicates the presence of the different functional groups. The peak observed in the higher energy region of intense absorption is 3487.00 cm<sup>-1</sup> which is characteristic of the stretching vibrations of O-H bonds in hydrogen-bonded hydroxyl (OH) groups, such as in alcohols or phenols. The peak at 2350.00 cm<sup>-1</sup> suggests the presence of a highly polarized bond, such as a triple bond (e.g., C≡N or C≡C) or nitriles. The peak at 1647.00 cm<sup>-1</sup> is often associated with the stretching vibrations of carbonyl groups (C=O) in compounds such as ketones and esters. The peak at 1082.00 cm<sup>-1</sup> region is commonly related to C-O stretching vibrations, which can be indicative of functional groups like alcohols, ethers, or esters. The peak at 798.85 cm<sup>-1</sup> region is often associated with the out-of-plane bending vibrations of aromatic (benzene-like) C-H bonds while the peak 459.00 in this region is typically in the fingerprint region, which contains a variety of small peaks unique to specific compounds.

PEMNPs have 17 peaks ranging from a wavelength of 3425.69 cm<sup>-1</sup> to 466.79 cm<sup>-1</sup>. The peak at 3425.69 cm<sup>-1</sup> is associated with the stretching vibrations of O-H bonds in hydrogen-bonded hydroxyl groups, which are commonly found in alcohols and phenols, the peak at 2426.53 cm<sup>-1</sup> and 2067.76 cm<sup>-1</sup> are characteristic of a triple bond, such as in a nitrile group (C≡N) or isocyanate (N=C=O), the peak at 1774.57 cm<sup>-1</sup> is typically associated with the stretching vibrations of carbonyl groups (C=O), suggesting the presence of a ketone or ester, the peak at 1639.55 cm<sup>-1</sup> is associated with C=C stretching vibrations in aromatic compounds or conjugated double bonds, the peak at 1508.38 cm<sup>-1</sup> is associated with aromatic ring vibrations, the peak at 1384.94 cm<sup>-1</sup> is associated with CH<sub>3</sub> bending vibrations, the peak at 1234.48 cm<sup>-1</sup> correspond to C-N stretching vibrations, possibly from an amine functional group, the peak at 1134.18 cm<sup>-1</sup> and 1072.46 cm<sup>-1</sup> are related to C-O stretching vibrations, indicating the presence of alcohols, ethers, or esters, the peak at 887.26 cm<sup>-1</sup> and 837.13 cm<sup>-1</sup> are associated with out-of-plane bending vibrations of aromatic (benzene-like) C-H bonds, the peak at 698.25 cm<sup>-1</sup> is related to out-of-plane bending vibrations of alkane C-H bonds, the peak at 597.95 cm<sup>-1</sup> is associated with out-of-plane bending vibrations of substituted aromatic rings, the peak at 536.23 cm<sup>-1</sup> region is associated with rocking vibrations of methylene (CH<sub>2</sub>) groups in alkanes, while the peak at 466.79 cm<sup>-1</sup> is associated with rocking vibrations of methyl (CH<sub>3</sub>) groups in alkanes.

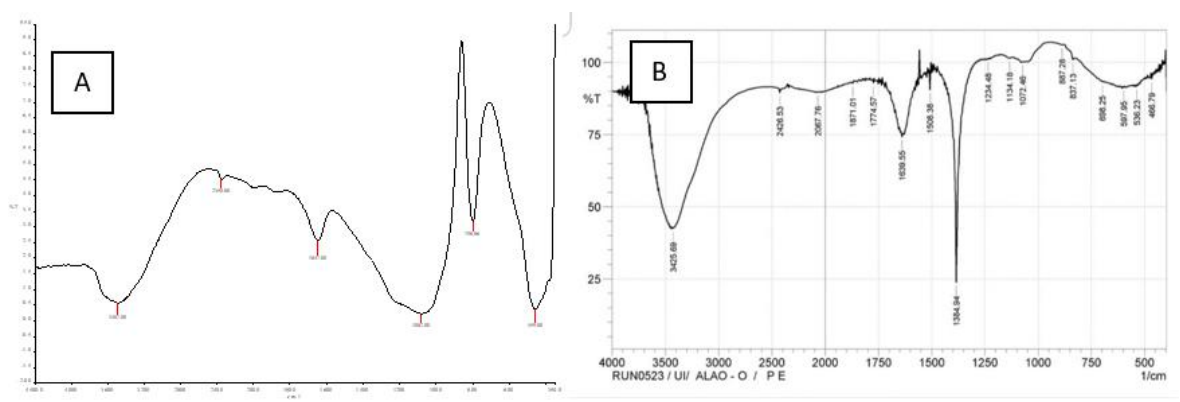
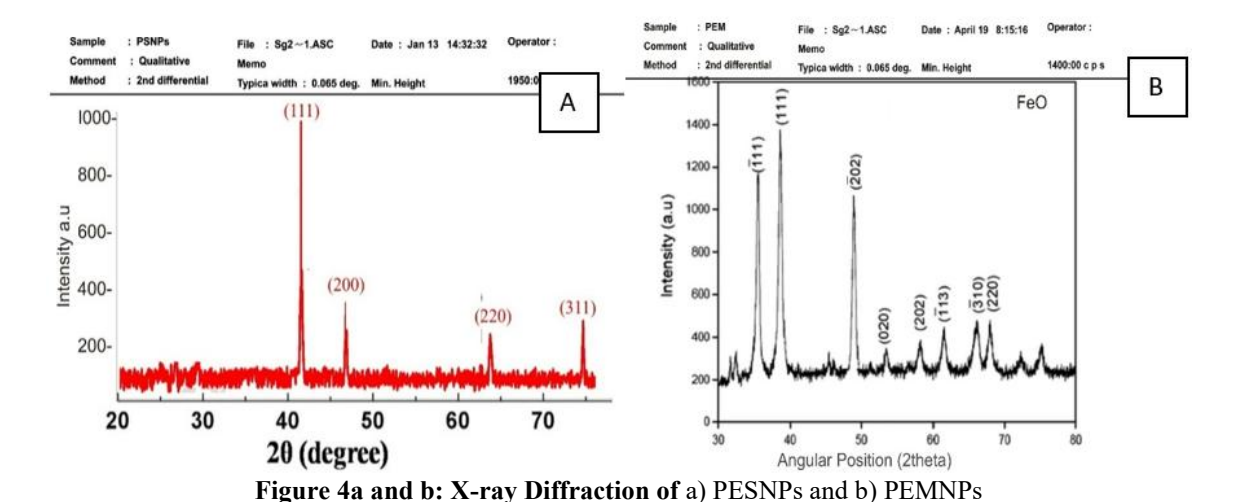


Figure 3a and b: Fourier Transform Infrared Spectroscopy (FTIR) of a) PESNPs and b) PEMNPs

The X-ray diffraction (XRD) analysis of the biosynthesized nanoparticles revealed distinctive patterns for both PESNPs and PEMNPs. For PESNPs, 4 prominent peaks were observed, with the maximum peak occurring at a  $2\theta$  value of  $40^\circ$ . This XRD pattern is illustrated in Figure 4a. In contrast, PEMNPs exhibited 8 peaks in their XRD pattern, with the maximum peak observed at a  $2\theta$  value of  $36^\circ$ . Figure 4b depicts the X-ray diffractogram (XRD) pattern for PEMNPs. These XRD patterns provide valuable insights into the crystalline structure of the synthesized nanoparticles, with the observed peaks corresponding to specific crystal planes within the nanoparticles.



The micrographs of PESNPs reveal relatively spherical nanoparticles with noticeable aggregation leading to the formation of larger clusters or nanoclusters. In contrast, the micrographs of PEMNPs depict an agglomeration structure morphology characterized by a uniform distribution of the particles. Figures 5a and 5b illustrate the scanning electron micrograph of the biosynthesized PESNPs and PEMNPs. These micrographs provide visual evidence of the distinct morphological characteristics of the silver and magnetic nanoparticles synthesized from the pawpaw seed extract.

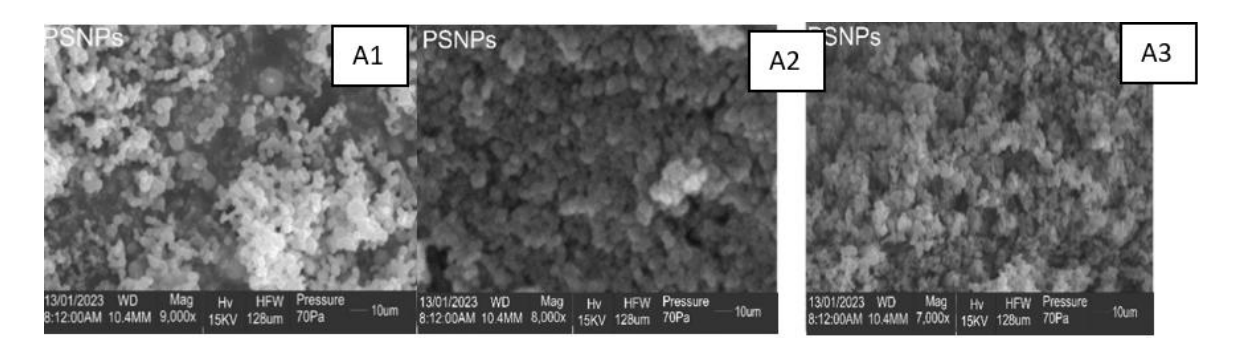


Figure 5a and b: Scanning Electron Microscopy (SEM) of a) PESNPs and b) PEMNPs

PESNPs range from 5-15 nm which appeared spherical in shape but with an increase in magnification, it has more of a rhombus-like shape. PEMNPs range from 20-80 nm and they appear circular but with uneven edges. Figure 6a and b shows the Transmission electron micrograph of the biosynthesized PESNPs and PEMNPs.

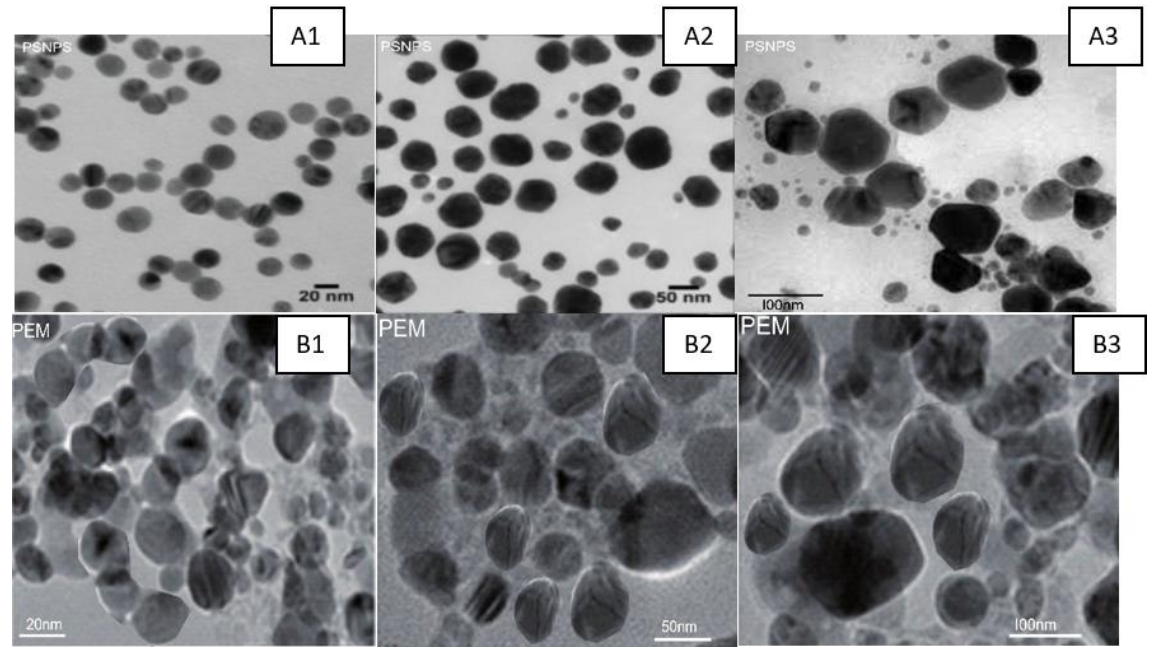


Figure 6a and b: Transmission Electron Microscopy (TEM) of a) PESNPs and b) PEMNPs

The elemental analysis of PESNPs and PEMNPs was revealed using Energy X-ray Spectroscopy (EDX) which is shown in Figures 7a and b. It was observed that PESNPs showed that silver was the most abundant element in the nanoparticle solution with 55.50% which is also a confirmation of the presence of silver nanoparticle production in the solution. Further peaks that were seen include C, O, N, Si, Mg, and Ca. PEMNPs, iron was observed to be the most abundant element with 63.34%. This shows the synthesis of magnetic nanoparticles. Further peaks that were seen include C, O, Na, S, and Si.

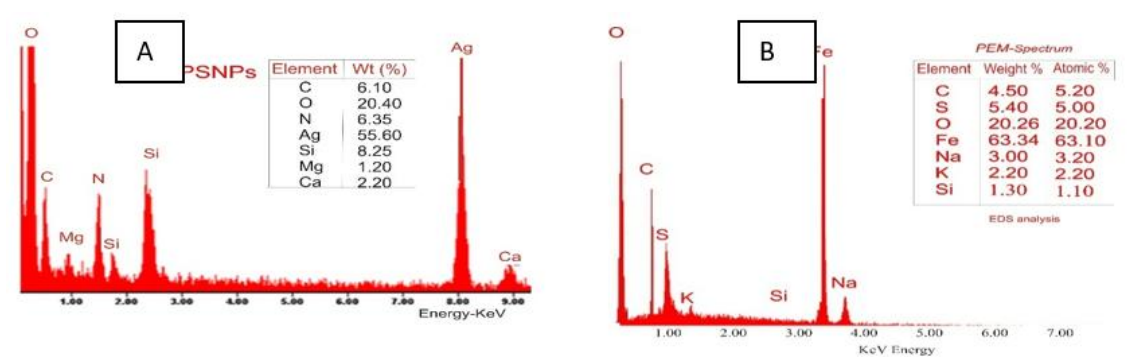


Figure 7a and b: EDX analysis of a) PESNPs and b) PEMNPs.

The thermal stability of PESNPs and PEMNPs about their weight was evaluated using Thermogravimetry (TGA). Figures 8a and b show that PESNPs were stable till 600°C with an 11.55% residue but with a lot of weight loss and PEMNPs were stable till 300°C, which shows that magnetic nanoparticles are less thermal stable than silver nanoparticles.

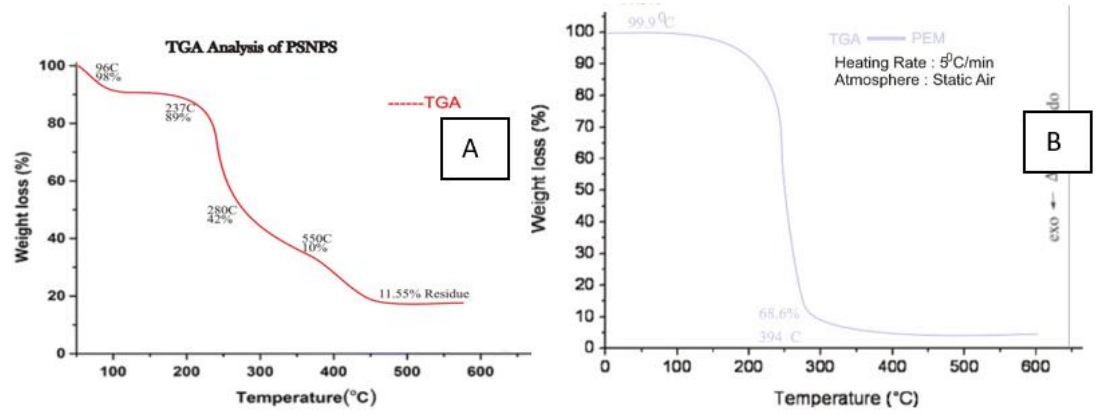


Figure 8a and b: TGA analysis of a) PESNPs and b) PEMNPs

The antibacterial activity of silver nanoparticles against test strains was determined as shown in Table 1. All the test isolates were susceptible to Alum and PESNPs while *Klebsiella pneumoniae* and *Salmonella typhimurium* were susceptible to PEMNPs. The antibacterial activity of PESNPs and PEMNPs ranged from 2.0 - 12.0 mm and 3.0 - 4.0 mm. *Salmonella typhimurium* had the highest susceptibility 12.0 mm and 4.0 mm for PESNPs and PEMNPs respectively.

Table 1: Antibacterial activity of the nanoparticles against some test pathogens isolated from wastewater samples

Isolate code	ALUM	PESNPs	PEMNPs	STREPTOMYCIN
Klebsiella pneumoniae	7.0	4.0	3.0	11.0
Salmonella typhimurium	7.0	12.0	4.0	14.0
Pseudomonas aeruginosa	8.0	6.0	0.0	16.0
E. coli 28	9.0	3.0	0.0	12.0
E. coli 27	8.0	2.0	0.0	14.0

The antibacterial activity of the nanoparticles against *Salmonella typhimurium* revealed that PESNPs exhibited the highest zone of inhibition (12mm) compared to the control.

Screening for the bio-flocculating potential of the plant extract and synthesized Silver and Iron nanoparticles is shown in Table 2. The bio-flocculating potential ranged from 50.10 to 84.20 % for nanoparticle samples at 12 hours and 54.10 to 87.80 % for nanoparticle samples at 24 hours. Notably, the highest bio-flocculating activity of 87.80 % was recorded for PESNPs at 24 hours.

Table 2: Bio-flocculating potential of the biosynthesized nanoparticles

Nanoparticle samples	Bioflocculating activity (%)		
	12hours	24hours	
ALUM	50.10	54.10	
PSE	62.96	78.37	
PESNPs	79.20	87.80	
PEMNPs	84.20	87.40	

The bioflocculating activities of the biosynthesized nanoparticles revealed that both PESNPs and PEMNPs exhibited high bioflocculating activities compared to their respective plant extracts. Interestingly, PEMNPs demonstrated a substantial level of potential, almost comparable to that of PESNPs.

Table 3 shows the Congo red and methylene blue reduction and oxidation potential of the biosynthesized PESNPs and PEMNPs. PESNPs exhibited 63.71 and 67.45 % reduction potential against Congo red and Methylene Blue respectively at 24 hours. PEMNPs had 31.40 and 39.52 % bi-oxidation potential against Congo red and Methylene Blue respectively at 24 hours. PESNPs had higher dye bio-reduction efficiency compared to PEMNPs.

Table 3: Dye reduction potential of the biosynthesized nanoparticle against Congo red and methylene blue

Nanoparticle samples	Dye Reduction (%) / Incubation Time (hrs.)				
	Conge	o Red	Methylene Blue		
	12 hrs.	24 hrs.	12 hrs.	24 hrs.	
PESNPs	33.71	63.71	37.41	67.45	
PEMNPs	21.00	31.40	26.00	39.52	

Untreated hospital wastewater carries high microbial loads, ranging from 36 to 91 x 10<sup>6</sup> CFU/mL, as shown in Table 4. Alum treatment reduces microbial load significantly (0–1 x 10<sup>6</sup> CFU/mL) by coagulating and removing microbes cost-effectively. PESNPs achieve complete microbial elimination (0 CFU/mL), while PEMNPs reduce the load moderately (3–32 x 10<sup>6</sup> CFU/mL), demonstrating varying antimicrobial efficiencies.

Table 4: Microbial load of untreated and treated hospital wastewater samples using PESNPs and PEMNPs

TREATMENT	SSA	EMB	MCA	NA NA
CONTROL	36	91	80	78
ALUM	-	1	-	-
PESNPs	-	-	-	-
PEMNPs	3	21	32	9

### IV. Discussion

This initial color change served as the primary indication that the methanolic extract of pawpaw seeds possesses the ability to bio-reduce silver nitrate (AgNO<sub>3</sub>) to generate silver nanoparticles (PESNPs) and bio-oxidize iron oxide (Fe<sub>2</sub>O<sub>3</sub>) to yield magnetic nanoparticles (PEMNPs). This color alteration was an evident and prominent characteristic of the nanoparticle synthesis process.

UV-Vis spectroscopy serves as a valuable technique for characterizing synthesized silver nanoparticles (AgNPs). In the case of *Papaya* extracts (PESNPs), the bio-reduction of silver nitrate leads to the biosynthesis of silver nanoparticles. Analysis of the absorption spectrum of the incubated solution across wavelengths ranging from 200 to 800 nm revealed a prominent peak at 500 nm. It's worth noting that the choice of precursor and the method employed for nanoparticle production play crucial roles in determining the characteristics of the synthesized nanoparticles, including their plasmon resonance (Narayanan et al., 2021). This observation aligns with the findings of Agustina et al. (2021), who studied the synthesis of silver nanoparticles using Diospyros maritima Blume leaves extract and reported an absorbance peak between 400 nm and 500 nm, indicative of AgNPs synthesis. They also noted that the absorption intensity of AgNPs increases with prolonged reaction time. Furthermore, Alharbi et al. (2022) suggested that broad and narrow peaks at higher and shorter wavelengths, respectively, indicate an increase or decrease in AgNP size. Adebayo-Tayo et al. (2019) reported similar findings, where they observed a Surface Plasmon Resonance (SPR) peak at 500 nm, with a broad spectrum ranging from 400 nm to 600 nm for biosynthesized silver nanoparticles using Oscillatoria sp. Regarding PEMNPs, the maximum absorbance peak was observed at 400 nm, consistent with the work of Ekwumemgbo et al. (2023), who detected a characteristic peak at 400 nm for Fe<sub>3</sub>O<sub>4</sub> nanoparticles using UV-vis spectroscopy. This finding also corresponds with the research of Sultana et al. (2023), who reported a maximum absorbance peak of 400 nm for iron nanoparticles synthesized from Catharanthus roseus leaf extract.

The FTIR analyses were conducted to characterize the silver and magnetic nanoparticles (NPs) and to investigate the potential bio-reducing functional groups present in PESNPs and PEMNPs. The spectrum of PESNPs was captured in the range of 459.00 to 3487.00 cm<sup>-1</sup>. The obtained FTIR results align with the findings of Aina et al. (2020), who synthesized silver nanoparticles from Carica papaya seeds. They observed that papaya seeds are abundant in sugars and unsaturated fatty acids but low in monosaccharide's. Similarly, Banala et al. (2015) conducted a study on the green synthesis and characterization of Carica papaya leaf extract-coated silver nanoparticles. They reported two sharp absorption peaks at 1640 cm<sup>-1</sup> and 3359 cm<sup>-1</sup>, indicating potential interactions between proteins and silver nanoparticles. These interactions could arise from the amide bonds present in proteins and the hydroxyl (OH) groups found in alcohols and phenolics, suggesting that these biomolecules play a role in capping and stabilizing the synthesized nanoparticles. On the other hand, the spectrum of PEMNPs was captured in the range of 3425.69 cm<sup>-1</sup> to 466.79 cm<sup>-1</sup>. This result is consistent with the work of Bhuiyan et al. (2020), who reported that shifts in peak positions within the range of 400–4000 cm<sup>-1</sup> indicate the presence of functional groups containing compounds bound to the iron oxide surface. Additionally, the peaks observed in this study resemble those reported in other studies on the biosynthesis of magnetite nanoparticles using Calotropis procera leaf extract by Kalu et al. (2022). The FTIR analyses provide insights into the functional groups present in PESNPs and PEMNPs, shedding light on the mechanisms involved in their synthesis and stabilization.

Using XRD pattern analysis, the crystal sizes of the silver and magnetic nanoparticles synthesized from *Papaya* extracts (PESNPs and PEMNPs) were investigated. The results revealed that the crystallite size of PESNPs and PEMNPs was approximately 54 nm and 38 nm respectively. These findings indicate that the silver nanoparticles formed through the reduction of Ag+ ions by the aqueous extract of *C. papaya* exhibited a crystalline structure. The presence of peaks in the XRD pattern suggests the involvement of a capping agent that aids in stabilizing the nanoparticles, as observed in previous studies (Balavijayalakshmi and Ramalakshmi, 2017). These results are consistent with the findings of Arokiyaraj *et al.* (2014), who reported similar peaks and a silver nanoparticle size of 53 nm when synthesizing silver nanoparticles using the marine algae *Padina pavonica*. Regarding the magnetic nanoparticles (PEMNPs), the XRD pattern indicated the formation of α-Fe<sub>2</sub>O<sub>3</sub> nanoparticles. The intense and sharp peaks observed confirmed the crystalline nature of the Fe<sub>2</sub>O<sub>3</sub> nanoparticles synthesized using *C. papaya* extract through the reduction method. These results are in agreement with previous studies conducted by Ahmmad *et al.* (2013), Suresh *et al.* (2016), and Bhuiyan *et al.* (2020), who also reported similar XRD patterns and crystallite sizes for iron oxide nanoparticles synthesized by various methods.

Scanning electron microscopy (SEM) analysis was conducted to examine the surface morphology and shapes of both silver and iron oxide nanoparticles. The SEM micrograph for PESNPs revealed the presence of spherical nanoparticles, with observable agglomeration leading to nanoparticle destabilization. This phenomenon of agglomeration aligns with previous findings reported by Narmadha *et al.* (2013). Additionally, Xia *et al.* (2018) explained that such agglomeration could be attributed to strong interparticle forces. On the other hand, the SEM micrograph for PEMNPs exhibited an agglomeration structure with a narrow distribution of particles, indicative of the magnetic characteristics of iron particles that allow for close contact with each other, as noted by Mohamed *et al.* (2023). Similar observations of agglomeration in iron oxide nanoparticles have been reported by Rahman *et al.* (2017) and Mahmoud *et al.* (2021), who attributed this phenomenon to the solution form of the sample and improper drying methods. Additionally, Wu *et al.* (2015) proposed that the presence of polyphenols in extracts could significantly influence the form and size of iron oxide nanoparticles, potentially contributing to their agglomeration.

TEM analysis provided insight into the sizes, shapes, and texture of both PESNPs and PEMNPs. The size of PESNPs ranged from 5 to 15  $\mu$ m, a finding consistent with the report of Madela (2019), who observed that biosynthesized silver nanoparticles typically exhibited small sizes with an average of 15 nm. In contrast, the size of PEMNPs ranged from 20 to 80  $\mu$ m, similar to the findings reported by Qais *et al.* (2019). It's noteworthy that magnetic nanoparticles were observed to be larger in size compared to the silver nanoparticles synthesized from the same plant extract. This observation aligns with the results reported by Chavan *et al.* (2020), who synthesized both silver and magnetic nanoparticles from *Blumea eriantha* plant extract and noted differences in size between the two nanoparticle types.

The EDX analysis revealed the presence of pure silver, iron, and other elements, confirming the successful biosynthesis of silver and iron nanoparticles. In the case of PESNPs, aside from silver, oxygen was also found to be abundant in the solution. This is likely attributed to the preparation process of silver nanoparticles, which involved the use of a distilled aqueous solution. Additionally, the presence of elements such as carbon (C), nitrogen (N), silicon (Si), magnesium (Mg), and calcium (Ca) suggests the utilization of a bio-flocculant, as these elements are commonly abundant in plants. Silicon, although less abundant, might have been introduced as an impurity. These elements likely served as capping organic agents bound to the surface of the silver nanoparticles, as reported by previous studies (Dada *et al.*, 2017; Femi-Adepoju *et al.*, 2019). Similarly, for PEMNPs, oxygen was the second most abundant element after iron. This observation aligns with the presence of oxygen in the synthesis process, likely originating from the aqueous environment. The presence of carbon and oxygen indicates the presence of polysaccharides and sugars in the plant extract, while the other elements are trace metals taken up by the plants, as reported by Mohammed *et al.* (2020) and Malaikozhundan *et al.* (2022). These findings highlight the complex interplay between the synthesis process, plant-derived components, and environmental factors in nanoparticle biosynthesis.

TGA analysis was conducted to assess the thermal stability, decomposition temperature, and decomposition rate of the nanoparticles (Bhuiyan *et al.*, 2020). The analysis of PESNPs revealed that they remain stable up to a temperature of 600°C, indicating minimal decomposition or weight loss in the silver nanoparticles. However, there was an observed residue of 11.55% at this temperature, suggesting the retention of mass, likely due to the presence of silver or other nanoparticle components. This finding is supported by Chen *et al.* (2016), who reported that silver nanoparticles exhibit high-temperature stability up to a certain threshold, after which sintering occurs, leading to nanoparticle coalescence and changes in morphology. In contrast, the analysis indicated that PEMNPs are stable only up to a temperature of 300°C, indicating lower thermal stability compared to silver nanoparticles. This lower stability suggests that magnetic nanoparticles begin to decompose or lose weight at a lower temperature compared to silver nanoparticles. Ansari *et al.* (2019) investigated the thermal stability and magnetic properties of iron oxide nanoparticles and found that while these

nanoparticles exhibit stability up to certain temperatures, beyond a critical temperature, there may be a decrease in magnetic properties due to structural changes or oxidation. Similarly, Wang *et al.* (2017) observed that some magnetic nanoparticles maintain stability at temperatures up to 300°C without significant degradation or loss of magnetic properties, but beyond this temperature, changes in nanoparticle morphology or magnetic behavior may occur, affecting their suitability for biomedical applications.

The antibacterial activity from this finding aligns with the results reported by Losasso *et al.* (2014), who demonstrated the effectiveness of silver nanoparticles against various serovars of *Salmonella* spp. Mikhailova *et al.* (2020) elucidated the mechanism of action of silver nanoparticles, suggesting that they may disrupt bacterial membranes, facilitating the entry of nanoparticles into the cell. Subsequent interactions with intracellular proteins and microbial DNA can interfere with cell division, ultimately leading to cell death. Furthermore, the results indicated that PESNPs exerted significantly greater antibacterial effects compared to PEMNPs. This observation is consistent with the findings of Gabrielyan *et al.* (2020), who reported that silver nanoparticles exhibit a more pronounced bactericidal effect than iron oxide nanoparticles. Similarly, Samadi *et al.* (2017) noted that while both types of nanoparticles possess antibacterial activity, silver nanoparticles are more effective than iron oxide nanoparticles.

The PESNPs and PEMNPs had high bioflocculating efficiency. Shende and Mitra (2021) proposed that this phenomenon could be attributed to the magnetic nanoparticles possessing a more positively charged ion (Fe<sup>3+</sup>) compared to silver (Ag<sup>2+</sup>), while most impurities exhibit a negative charge. This difference in charge facilitates the formation of flocs by magnetic nanoparticles more effectively than silver nanoparticles' bioflocculants

The dye reduction potential of PESNPs revealed that both at 12 hours and 24 hours, silver nanoparticles exhibited a high dye-reducing capacity for both Congo red and methylene blue. This phenomenon may be attributed to the presence of phytochemicals and antioxidant properties inherent in both silver nanoparticles and pawpaw seed extract. It is noteworthy that Congo red was more effectively reduced, possibly due to its propensity to aggregate in the presence of silver ions. This observation aligns with the findings of Riaz *et al.* (2020), who utilized silver nanoparticles in the reduction of Congo red. The bond dissociation energy (BDE) plays a crucial role in chemical reactions by facilitating the breaking and/or formation of new bonds. During this process, electron transfer occurs, with methylene blue in the solution serving as the electron acceptor while silver nanoparticles act as the electron donor. The more electrons accepted from the silver nanoparticles, the greater the reduction in the amount of methylene blue. This mechanism is supported by the studies of Vanaja *et al.* (2014) and Saha *et al.* (2017).

High microbial loads in untreated wastewater loaded with pathogens and resistant strain poses a health risk (Bárbara et al., 2019; Kaur et al., 2020). These findings stress the need for effective hospital wastewater treatment to mitigate risks (Majumder et al., 2021). Combining traditional methods like alum with advanced nanoparticle technology offers promising solutions to better remove pathogens and antibiotic resistance before environmental discharge (Todedji et al., 2020; Yuan and Pian, 2023).

# V. Conclusion

Green synthesis of silver and iron nanoparticles using *C. papaya* extracts offers an eco-friendly approach for biological applications. Characterization of papaya-derived silver (PESNPs) and magnetic (PEMNPs) nanoparticles reveals their stability, synthesis mechanisms, and functionality. PESNPs show strong antimicrobial activity against *Salmonella typhimurium*, while both nanoparticles demonstrate effective bio-flocculating properties. These nanoparticles offer eco-friendly alternatives for water treatment, including industrial wastewater purification and dye removal. The study highlights their broad potential in biomedicine, environmental science, and nanotechnology

#### References

- [1]. Agustina TE, Handayani W, Imawan C. The UV-Vis Spectrum Analysis From Silver Nanoparticles Synthesized Using Diospyros Maritima Blume Leaves Extract. Advances In Biological Sciences Research. 2021;14:411-419.
- [2]. Adebayo-Tayo B, Salaam A, Ajibade A. Green Synthesis Of Silver Nanoparticle Using Oscillatoria Sp. Extract, Its Antibacterial, Antibiofilm Potential And Cytotoxicity Activity. Heliyon. 2019;5(10):02502.
- [3]. Adebayo-Tayo BC, Adeleke RO, Adekanmbi AO. Biogenic Silver And Magnetic Nanoparticles Using Bacillus Subtilis B2 Bioflocculants; Production, Properties And Antibacterial Potential In Dairy Wastewater Treatment. Chemistry Africa. 2022;5(5):1547-1561.
- [4]. Adekanmbi A, Adejoba AT, Banjo OA, Saki M. Detection Of Sul1 And Sul2 Genes In Sulfonamide-Resistant Bacteria (SRB) From Sewage, Aquaculture Sources, Animal Wastes And Hospital Wastewater In South-West Nigeria. Gene Reports. 2020;20:100742-100747.
- [5]. Ahmmad B, Leonard K, Islam MS, Kurawaki J, Muruganandham M, Ohkubo T, Kuroda Y. Green Synthesis Of Mesoporous Hematite (A-Fe2O3) Nanoparticles And Their Photocatalytic Activity. Advanced Powder Technology. 2013;24(1):160-167.
- [6]. Aina AD, Owolo O, Adeoye-Isijola M, Olukanni OD, Lateef A, Egbe T, Aina FO, Asafa TB, Abbas SH. Ecofriendly Production Of Silver Nanoparticles From The Seeds Of Carica Papaya And Its Larvicidal And Antibacterial Efficacy Against Some Selected Bacterial Pathogens. IOP Conference Series: Materials Science And Engineering. 2020;805(1):012038.

- [7]. Alharbi SN, Alsubhi SN, Felimban AI. Green Synthesis Of Silver Nanoparticles Using Medicinal Plants: Characterization And Application. Journal Of Radiation Research And Applied Sciences. 2022;15(3):109-124.
- [8]. Abdallah N, Ahmed S, Hassan S. Characterization Of Silver Nanoparticles Synthesized Using Plant Extracts. Biointerface Research In Applied Chemistry. 2020;10(6):7260-7269.
- [9]. Ansari S, Ficiarà E, Ruffinatti F, Stura I, Argenziano M, Abollino O, Cavalli R, Guiot C, D'Agata F. Magnetic Iron Oxide Nanoparticles: Synthesis, Characterization And Functionalization For Biomedical Applications In The Central Nervous System. Materials. 2019;12(3):465.
- [10]. Aravind G, Debjit B, Duraivel S, Harish G. Traditional And Medicinal Uses Of Carica Papaya. Journal Of Medicinal Plants Studies. 2013;1(1):7-15.
- [11]. Arokiyaraj S, Arasu MV, Vincent S, Oh YK, Kim KH, Choi KC, Choi SH, Prakash NU. Rapid Green Synthesis Of Silver Nanoparticles From Chrysanthemum Indicum L. And Its Antibacterial And Cytotoxic Effects: An In Vitro Study. International Journal Of Nanomedicine. 2014;379.
- [12]. Aromal SA, Philip D. Green Synthesis Of Gold Nanoparticles Using Trigonella Foenum Graecum And Its Size Dependent Catalytic Activity. Spectrochimica Acta Part A: Molecular And Biomolecular Spectroscopy. 2012;97:1-5.
- [13]. Balavijayalakshmi J, Ramalakshmi V. Carica Papaya Peel Mediated Synthesis Of Silver Nanoparticles And Its Antibacterial Activity Against Human Pathogens. Journal Of Applied Research And Technology. 2017;15(5):413-422.
- [14]. Banala RR, Nagati VB, Karnat PR. Green Synthesis And Characterization Of Carica Papaya Leaf Extract Coated Silver Nanoparticles Through X-Ray Diffraction, Electron Microscopy And Evaluation Of Bactericidal Properties. Saudi Journal Of Biological Sciences. 2015;22(5):637-644.
- [15]. Bar H, Bhui DK, Sahoo GP, Sarkar P, De PS, Misra A. Green Synthesis Of Silver Nanoparticles Using Latex Of Jatropha Curcas. Colloids And Surfaces A: Physicochemical And Engineering Aspects. 2009;339(3):134-139.
- [16]. Bharathi D, Josebin MD, Bhuvaneshwari V. Biosynthesis Of Silver Nanoparticles Using Stem Bark Extracts Of Diospyros Montana And Their Antioxidant And Antibacterial Activities. Journal Of Nanostructure In Chemistry. 2018;8(1):83-92.
- [17]. Bhuiyan SH, Miah MY, Paul SC, Aka T, Saha O, Rahaman M, Sharif JI, Habiba O, Ashaduzzaman M. Green Synthesis Of Iron Oxide Nanoparticles Using Carica Papaya Leaf Extract: Application For Photocatalytic Degradation Of Remazol Yellow RR Dye And Antibacterial Activity. Heliyon. 2020;6(8):E04603.
- [18]. Chavan RR, Bhinge SD, Bhutkar MA, Randive DS, Wadkar GH, Todkar SS, Urade MN. Characterization, Antioxidant, Antimicrobial, And Cytotoxic Activities Of Green Synthesized Silver And Iron Nanoparticles Using Alcoholic Blumea Eriantha DC Plant Extract. Materials Today Communications. 2020;24:101320.
- [19]. Chen H, Ohodnicki P, Baltrus JP, Holcomb G, Tylczak J, Du H. High-Temperature Stability Of Silver Nanoparticles Geometrically Confined In The Nanoscale Pore Channels Of Anodized Aluminum Oxide For SERS In Harsh Environments. RSC Advances. 2016;6(90):86930-86937.
- [20]. Cruz D, Falé PL, Mourato A, Vaz PD, Serralheiro MI, Lino ARL. Preparation And Physicochemical Characterization Of Ag Nanoparticles Biosynthesized By Lippia Citriodora (Lemon Verbena). Colloid And Surface B: Biointerfaces. 2010;81:67-73.
- [21]. Dada AO, Adekola FA, Odebunmi EO. A Novel Zerovalent Manganese For Removal Of Copper Ions: Synthesis, Characterization And Adsorption Studies. Applied Water Science. 2017;7(3):1409-1427.
- [22]. Dash A, Ahmed MT, Selvaraj R. Mesoporous Magnetite Nanoparticles Synthesis Using The Peltophorum Pterocarpum Pod Extract, Their Antibacterial Efficacy Against Pathogens And Ability To Remove A Pollutant Dye. Journal Of Molecular Structure. 2019;1178:268-273.
- [23]. Dhar KP, Saha P, Hasan K, Amin R, Haque. Green Synthesis Of Magnetite Nanoparticles Using Lathyrus Sativus Peel Extract And Evaluation Of Their Catalytic Activity. Cleaner Engineering And Technology. 2021;3:100117.
- [24]. Dharshini RS, Poonkothai M, Srinivasan P, Mythili R, Syed A, Elgorban AM, Selvankumar T, Kim W. Nano-Decolorization Of Methylene Blue By Phyllanthus Reticulatus Iron Nanoparticles: An Eco-Friendly Synthesis And Its Antimicrobial, Phytotoxicity Study. Applied Nanoscience. 2021;21:1-11.
- [25]. Dlamini SB, Zuniga JS, Lakshmanan R. Role Of Magnetic Nanoparticles In Wastewater Treatment: An Overview. Journal Of Environmental Management. 2020;265:110525.
- [26]. Ekwumemgbo AP, Shallangwa GA, Okon EI. Green Synthesis And Characterization Of Iron Oxide Nanoparticles Using Prosopis Africana Leaf Extract. Communication In Physical Sciences. 2023;9(2):125-136.
- [27]. Femi-Adepoju AG, Dada AO, Otun KO, Adepoju AO, Fatoba OP. Green Synthesis Of Silver Nanoparticles Using Terrestrial Fern (Gleichenia Pectinata (Willd.) C. Presl.) Characterization And Antimicrobial Studies. Heliyon. 2019;5(4):E01543.
- [28]. Gabrielyan L, Badalyan H, Gevorgyan V, Trchounian A. Comparable Antibacterial Effects And Action Mechanisms Of Silver And Iron Oxide Nanoparticles On Escherichia Coli And Salmonella Typhimurium. Scientific Reports. 2020;10(1):13145.
- [29]. Groiss S, Selvaraj R, Thivaharan V, Ramesh V. Structural Characterization, Antibacterial And Catalytic Effect Of Iron Oxide Nanoparticles Synthesized Using The Leaf Extract Of Cynometra Ramiflora. Journal Of Molecular Structure. 2017;1128:572-578.
- [30]. Kadry MS. Antioxidant And Immunostimulant Effect Of Carica Papaya Linn Aqueous Extract In Acrylamide Intoxicated Rats. Acta Informatica Medica. 2012;20(3):180-185.
- [31]. Kaur R, Yadav B, Tyagi RD. Microbiology Of Hospital Wastewater. Current Developments In Biotechnology And Bioengineering. 2020;103-148.
- [32]. Kalu AO, Egwin EC, Jigam AA, Muhammed HL. Green Synthesis Of Magnetite Nanoparticles Using Calotropis Procera Leaf Extract And Evaluation Of Its Antimicrobial Activity. Nanoexpress. 2022;3:045004.
- [33]. Kuppusamy P, Yusoff MM, Maniam GP, Govindan N. Biosynthesis Of Metallic Nanoparticles Using Plant Derivatives And Their New Avenues In Pharmacological Applications An Updated Report. Saudi Pharmaceutical Journal. 2016;24(4):473–484.
- [34]. Losasso C, Belluco S, Cibin V, Zavagnin P, Mičetić I, Gallocchio F, Zanella M, Bregoli L, Biancotto G, Ricci A. Antibacterial Activity Of Silver Nanoparticles: Sensitivity Of Different Salmonella Serovars. Frontiers In Microbiology. 2014;26(5):227.
- [35]. Madela M. Impact Of Silver Nanoparticles On Wastewater Treatment In The SBR. E3S Web Of Conferences. 2019;86:0002.
- [36]. Majumder A, Gupta AK, Ghosal PS, Varma M. A Review On Hospital Wastewater Treatment: A Special Emphasis On Occurrence And Removal Of Pharmaceutically Active Compounds, Resistant Microorganisms, And SARS-Cov-2. Journal Of Environmental Chemical Engineering. 2021;9(2):104812.
- [37]. Mahmoud R, Kotp AA, El-Ela FIA, Farghali AA, Moaty SA, Zahran HY, Amin R. Green Synthesis Of Iron Nanoparticles Of Clove And Green Coffee Origin With An In Vivo Hepatoprotective Investigation. Journal Of Environmental Chemical Engineering. 2021;9(6):106320.
- [38]. Malaikozhundan B, Krishnamoorthi R, Vinodhini J, Nambi KSN, Palanisamy S. Multifunctional Iron Oxide Nanoparticles Using Carica Papaya Fruit Extract As Antibacterial, Antioxidant And Photocatalytic Agent To Remove Industrial Dyes. Inorganic Chemistry Communications. 2022;144:109843.

- [39]. Mikhailova EO. Silver Nanoparticles: Mechanism Of Action And Probable Bio-Application. Journal Of Functional Biomaterials. 2020;11(4):84.
- [40]. Mohamed A, Atta RR, Kotp AA, Abo El-Ela FI, Abd El-Raheem H, Farghali A, Alkhalifah DHM, Hozzein WN, Mahmoud R. Green Synthesis And Characterization Of Iron Oxide Nanoparticles For The Removal Of Heavy Metals (Cd2+ And Ni2+) From Aqueous Solutions With Antimicrobial Investigation. Scientific Reports. 2023;13(1):7227.
- [41]. Mohammed AYA, Bady ZAM, Fahmy AM, Ahmed AM. Investigation Of The Potential Of Opuntia Ficus-Indica Powder For Sewage Treatment. International Journal Of Scientific And Research Publications. 2020;3:20-45.
- [42]. Mulvaney P. Surface Plasmon Spectroscopy Of Nanosized Metal Particles. Langmuir. 1996;12(3):788-800.
- [43]. Narayanan M, Divya S, Natarajan D, Senthil-Nathan S, Kandasamy S, Chinnathambi A, Alahmadi TA, Pugazhendhi A. Green Synthesis Of Silver Nanoparticles From Aqueous Extract Of Ctenolepis Garcini L. And Assess Their Possible Biological Applications. Process Biochemistry. 2021;107:91-99.
- [44]. Narmadha E, Hemashenpagam N, Sathiya SV, Vasantha SR. Characterization Of Papaya Fruit-Mediated Silver Nanoparticles And Evaluation Of Its Antimicrobial And Wound Healing Activity. International Research Journal Of Pharmacy. 2013;4:166-169.
- [45]. Nkosinathi DG, Albertus BK, Jabulani SS, Siphephelo S, Pullabhotla RV. Biosynthesis, Characterization, And Application Of Iron Nanoparticles: In Dye Removal And As Antimicrobial Agent. Water, Air, And Soil Pollution. 2020;231:1-10.
- [46]. Qais FA, Shafiq A, Khan HM, Husain FM, Khan RA, Alenazi B, Alsalme A, Ahmad I. Antibacterial Effect Of Silver Nanoparticles Synthesized Using Murraya Koenigii (L.) Against Multidrug-Resistant Pathogens. Bioinorganic Chemistry And Applications. 2019;6:56-63.
- [47]. Rahman SSU, Qureshi MT, Sultana K, Rehman W, Khan MY, Asif MH, Farooq M, Sultana N. Single Step Growth Of Iron Oxide Nanoparticles And Their Use As Glucose Biosensor. Results In Physics. 2017;7:4451-4456.
- [48]. Raina S, Roy A, Bharadvaja N. Degradation Of Dyes Using Biologically Synthesized Silver And Copper Nanoparticles. Environmental Nanotechnology, Monitoring And Management. 2020;13:100278.
- [49]. Riaz M, Ismail M, Ahmad B, Zahid N, Jabbour G, Khan MS, Mutreja V, Sareen S, Rafiq A, Faheem M, Shah MM. Characterizations And Analysis Of The Antioxidant, Antimicrobial, And Dye Reduction Ability Of Green Synthesized Silver Nanoparticles. Green Processing And Synthesis. 2020;9(1):693-705.
- [50]. Saba S, Pattan N. The Potential Health Benefits Of Papaya Seeds. International Journal For Research In Applied Science And Engineering Technology. 2022;10:44-50.
- [51]. Saha J, Begum A, Mukherjee A, Kumar S. A Novel Green Synthesis Of Silver Nanoparticles And Their Catalytic Action In Reduction Of Methylene Blue Dye. Sustainable Environment Research. 2017;27(5):245-250.
- [52]. Samadi S, Meshkini A, Kowsari K. Antibacterial Activity Of Silver Nanoparticles And Iron Oxide Nanoparticles Against Staphylococcus Aureus And Escherichia Coli. International Journal Of Nanomedicine. 2017;12:4791-4800.
- [53]. Shende AP, Mitra N. Green Synthesis Of Iron Nanoparticles Using Bioflocculant Extracted From Okra (Abelmoschus Esculentus (L) Moench) And Its Application Towards Elimination Of Toxic Metals From Wastewater: A Statistical Approach. Journal Of Water And Environmental Nanotechnology. 2021.
- [54]. Sinhalagoda LC, Susiji W, Roshitha NW, Rajapakse PV, Senanayake AM. Does Carica Papaya Leaf-Extract Increase The Platelet Count? An Experimental Study In A Murine Model. Asian Pacific Journal Of Tropical Biomedicine. 2013;3(9):720-724.
- [55]. Sultana MJ, Nibir AS, Ahmed FR. Biosensing And Anti-Inflammatory Effects Of Silver, Copper And Iron Nanoparticles From The Leaf Extract Of Catharanthus Roseus. Beni-Suef University Journal Of Basic And Applied Sciences. 2023;12(1):2-7.
- [56]. Suryawanshi P, Vidyasagar GM. Biosynthesis Of Silver Nanoparticles From Three Opuntia Spp. International Journal Of Advanced Scientific Research And Management. 2019;4(7).
- [57]. Suresh S, Karthikeyan S, Jayamoorthy K. Effect Of Bulk And Nano-Fe2O3 Particles On Peanut Plant Leaves Studied By Fourier Transform Infrared Spectral Studies. Journal Of Advanced Research. 2016;7(5):739-747.
- [58]. Todedji J, Degbey C, Soclo E, Yessoufou A, Hounfodji J, Goudjo F, Suanon F, Mama D. Microbiological Quality Of The Effluents Produced By The University And Hospital Centres In The Department Of Littoral, Republic Of Benin. Open Journal Of Epidemiology. 2020;10:66-80.
- [59]. Vanaja M, Paulkumar K, Baburaja M, Rajeshkumar S, Gnanajobitha G, Malarkodi C, Sivakavinesan M, Annadurai G. Degradation Of Methylene Blue Using Biologically Synthesized Silver Nanoparticles. Bioinorganic Chemistry And Applications. 2014;33(9):101-132.
- [60]. Wu JY, Ye HF. Characterization And Flocculating Properties Of An Extracellular Biopolymer Produced From Bacillus Subtilis DYU1 Isolate. Process Biochemistry. 2007;42(7):1114-1123.
- [61]. Wang F, Yang Y, Ling Y, Liu J, Cai X, Zhou X, Tang X, Liang B, Chen Y, Chen H, Chen D, Li C, Wang Z, Hu B, Zheng Y. Injectable And Thermally Contractible Hydroxypropyl Methyl Cellulose/Fe3O4 For Magnetic Hyperthermia Ablation Of Tumors. Biomaterials. 2017;128:84-93.
- [62]. Wu Y, Zeng S, Wang F, Megharaj M, Naidu R, Chen Z. Heterogeneous Fenton-Like Oxidation Of Malachite Green By Iron-Based Nanoparticles Synthesized By Tea Extract As A Catalyst. Separation And Purification Technology. 2015;154:161-167.
- [63]. Xia X, Lan S, Li X, Xie Y, Liang Y, Yan P, Chen Z, Xing Y. Characterization And Coagulation-Flocculation Performance Of A Composite Flocculant In High-Turbidity Drinking Water Treatment. Chemosphere. 2018;206:701-708.
- [64]. Yuan T, Pian Y. Hospital Wastewater As Hotspots For Pathogenic Microorganisms Spread Into Aquatic Environment: A Review. Frontiers In Environmental Science. 2023;10:1091734.
- [65]. Bárbara WN Grehs, Ana Rita Lopes, Nuno FF Moreira, Telma Fernandes, Maria AO Linton, Adrián MT Silva, Célia M Manaia, Elvis Carissimi, Olga C Nunes. Removal Of Microorganisms And Antibiotic Resistance Genes From Treated Urban Wastewater: A Comparison Between Aluminium Sulphate And Tannin Coagulants. Water Research. 2019;166:115056.
- [66]. Kaur R, Yadav B, Tyagi RD. Microbiology Of Hospital Wastewater. Current Developments In Biotechnology And Bioengineering. 2020;103-148.
- [67]. Majumder A, Gupta AK, Ghosal PS, Varma M. A Review On Hospital Wastewater Treatment: A Special Emphasis On Occurrence And Removal Of Pharmaceutically Active Compounds, Resistant Microorganisms, And SARS-Cov-2. Journal Of Environmental Chemical Engineering. 2021;9(2):104812.
- [68]. Adekanmbi A, Adejoba AT, Banjo OA, Saki M. Detection Of Sul1 And Sul2 Genes In Sulfonamide-Resistant Bacteria (SRB) From Sewage, Aquaculture Sources, Animal Wastes And Hospital Wastewater In South-West Nigeria. Gene Reports. 2020;20:100742-100747.
- [69]. Todedji J, Degbey C, Soclo E, Yessoufou A, Hounfodji J, Goudjo F, Suanon F, Mama D. Microbiological Quality Of The Effluents Produced By The University And Hospital Centres In The Department Of Littoral, Republic Of Benin. Open Journal Of Epidemiology. 2020;10:66-80.